Plasmonics (2025) 20:1721–1728
https://doi.org/10.1007/s11468-024-02354-w

RESEARCH

Modeling a Graphene-Enhanced Surface Plasmon Resonance Sensor for Cancer Detection

Sahar Abdalla[1,2] · Hela Ferjani[1] · Ahmad M. Alsaad[3,4] · Carlos J. Tavares[5] · Ahmad D. Telfah[6,7]

Received: 28 March 2024 / Accepted: 13 May 2024 / Published online: 26 June 2024
© The Author(s), under exclusive licence to Springer Science+Business Media, LLC, part of Springer Nature 2024

Abstract
This study presents an innovative surface plasmon resonance (SPR) biosensor model constructed with a glass prism coated first with a layer of silver followed by a graphene layer (glass prism/Ag/graphene). The biosensor was analyzed using a finite element method-based simulation platform. Evaluation of the SPR sensor was conducted using a range of normal and cancer cell lines, including Basal (skin cancer), HeLa (cervical cancer), Jurkat (blood cancer), PC12 (adrenal gland cancer), and MCF-7 (breast cancer) cells. The results demonstrate the biosensor's effectiveness in detecting various cancerous cells across a wide range of refractive index variations. Sensitivity values for skin, cervical, blood, adrenal gland, and breast cancer cells are reported as 120.0 °/RIU, 200.0 °/RIU, 142.9 °/RIU, 114.3 °/RIU, and 114.3 °/RIU, respectively. This proposed biosensor model offers significant potential for a variety of bio-sensing applications.

Keywords Surface plasmon resonance · Biosensors · Refractive index · Cancerous cells

Introduction

Early cancer detection is essential for effective treatment [1, 2]. Common types of cancer include Jurkat (blood cancer), HeLa (cervical cancer), PC12 (adrenal gland cancer), MCF-7 (breast cancer - type 2), and Basal (skin cancer) [3, 4], often exhibiting high viability rates exceeding 70% [5]. As cancer cells proliferate, they undergo changes in their refractive index [6], which can be leveraged by early detection methods. Understanding the optical properties of cancer cells is therefore crucial for improving cancer diagnosis and treatment.

Optical biosensors demonstrate powerful sensing capabilities, showing high sensitivity to changes in the optical parameters of tested media [7]. Surface Plasmon Resonance (SPR) is a label-free sensing technique particularly suited for bio-detection, enabling real-time, reproducible, and cost-effective measurements of biomolecule binding kinetics and affinity [8, 9]. SPR is highly suitable for virus detection due to its ability to eliminate weakened binding issues observed with labeled techniques, relying on variations in refractive index of biological solutions or chemical analytes [10–12]. SPR biosensors rely on refractive index variations induced by objects near a metal surface irradiated with monochromatic light, monitoring shifts in incident angle to plot real-time response curves [13, 14].

SPR biosensors can utilize metals like gold (Au), silver (Ag), and copper (Cu) for the sensitive layer [15]. Silver (Ag) offers advantages including small optical damping, absence of interband transfer at visible light frequencies, sharper resonance peaks, and narrower SPR curves [16–18]. Graphene, known for its excellent conductivity and effective biomolecule adsorption capabilities, shows promise in biosensor applications [19, 20], with π-stacking interactions enhancing its suitability for various applications including

✉ Ahmad D. Telfah
ahmad.telfah@fh-dortmund.de

Sahar Abdalla
SSAbdalla@imamu.edu.sa

1 Chemistry Department, College of Science, Imam Mohammad Ibn Saud Islamic University (IMSIU), Riyadh 11623, Saudi Arabia

2 Department of Chemistry, Faculty of Science, University of Khartoum, P.O. Box 321, Khartoum, Sudan

3 Department of Physical Sciences, Jordan University of Science & Technology, Irbid 22110, Jordan

4 Department of Physics, University of Nebraska at Omaha, Omaha NE-68182, USA

5 Centre of Physics of Minho and Porto Universities (CF-UM-UP), University of Minho, Guimarães 4804-533, Portugal

6 Fachhochschule Dortmund – University of Applied Sciences and Arts, Sonnenstrasse 96-100, 44139 Dortmund, Germany

7 Cell Therapy Center, The University of Jordan, 11942 Amman, Jordan

optical, electrochemical, and biosensing [12, 21–23]. Additionally, the primary challenge of silver layer oxidation is addressed by using graphene layers to protect the silver layer, thereby improving sensitivity.

This study aims to develop a cancer bio-detector based on Surface Plasmon Resonance (SPR) to detect refractive index variations in cancer cells for early detection. We analyze the performance of the proposed SPR sensor, consisting of a Prism/Ag/graphene configuration, using finite element method (FEM) simulations. Our approach utilizes advanced FEM-based numerical methods to model a highly sensitive hybrid SPR-based biosensor for cancer cell detection. We assess the effectiveness of this model SPR sensor in detecting various types of cancer cells, including skin (basal), cervical (HeLa), adrenal gland (PC12), blood (Jurkat), and breast (MCF-7) cancer cells. The results and interpretations derived from this model SPR sensor will guide future experimental approaches toward developing practical sensors based on promising numerical simulations.

Methods

Sensor Structural Design

The SPR biosensor is configured in the Kretschmann arrangement, featuring a glass prism coated with a silver layer of optimal thickness ranging from 20 to 40 nm, followed by a functionalized graphene layer approximately 0.34 nm thick deposited on top of the silver layer. This configuration is represented as glass prism/Ag/graphene, as illustrated in Fig. 1 [24]. The sensor operates at a monochromatic wavelength of 633 nm, utilizing a He-Ne laser [25].

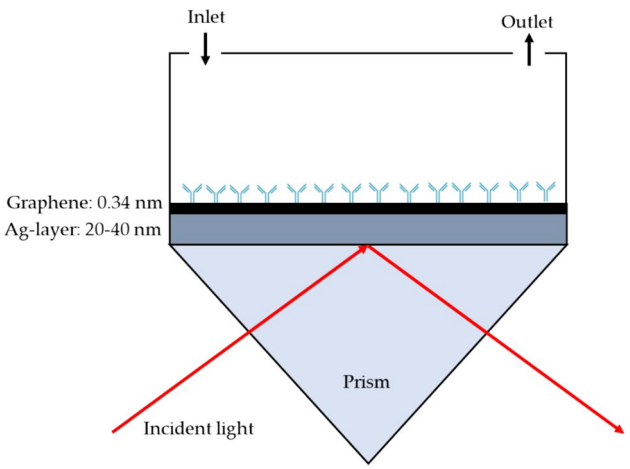


Fig. 1 Schematic representation of the glass prism/Ag/graphene SPR biosensor configured in the Kretschmann arrangement

Table 1 shows the key parameters of the modeled glass prism/Ag/graphene SPR biosensor.

A π-polarized light with a wavelength (λ) of 633 nm was incident at the appropriate angle on a glass prism, utilizing angular interrogation to determine the resonance angle. At resonance, the reflectance intensity reaches its minimum as the light wave passes through the interfaces of the Ag and graphene layers, resulting in reduced reflection intensity at the output. Monitoring of the output reflectance intensity can be achieved using CCD or CMOS image sensors [25].

Theoretical Model

Surface plasmon waves (SPWs) consist of transverse oscillating electric fields perpendicular to the surface. The transverse magnetic (TM) polarization state occurs when the surface plasmon propagates parallel to the x-axis with a magnetic field directed along the y-axis. This TM polarization state is crucial for inducing charge distribution on the metal contact [28, 29]. When light passes through the Ag layer, π-polarized SPR waves are generated at the interface between the metal and dielectric media.

The SPWs propagating along the (x, 0, z) direction can be described mathematically as follows:

$$E_i(\vec{r},t) = \left(E_{ix}, 0, E_{iz}\right)\left[e^{-|Z|k_{iz}}e^{i\left(xk_{ix}-\omega t\right)}\right] \tag{1}$$

$$H_i(\vec{r},t) = \left(0, H_{iy}, 0\right)\left[e^{-|Z|k_{iz}}e^{i\left(xk_{ix}-\omega t\right)}\right] \tag{2}$$

In these equations, ω represents the frequency, E denotes the electric field vector, H signifies the magnetic field vector, k_{iz} and k_{ix} represent the z and $x$components of the wave vector, respectively. By applying the continuity conditions,

$$k_{iz} = \sqrt{\epsilon_i\left(\frac{\omega}{c}\right)^2 - k_{ix}^2} \tag{3}$$

and,

$$\frac{k_{z1}}{\epsilon_m}H_{1y} + \frac{k_{z2}}{\epsilon_d}H_{2y} = 0 \tag{4}$$

$$H_{1y} - H_{2y} = 0 \tag{5}$$

Table 1 Key parameters of the modeled glass prism/Ag/graphene SPR biosensor

Layer	Optimum Thickness	Refractive index (real part)	Refractive index (imaginary part)
Prism	--	1.72	--
Ag [26]	20–60	0.056	4.835
Graphene [27]	0.340	3.00	1.149

When the determinant equals zero, the equation can be expressed as:

$$k_{z1}\epsilon_d + k_{z2}\epsilon_m = 0 \tag{6}$$

At $K_{x1} = K_{x2} = K_x$, the expression becomes:

$$K_x = \frac{\omega}{c}\sqrt{\frac{\epsilon_m \epsilon_d}{\epsilon_m + \epsilon_d}} \tag{7}$$

Equation (7) describes the surface plasmon wave vector $K_x = K_{sp}$, representing the generation of surface plasmons. Here, ϵ_m and ϵ_d denote the dielectric constants of the metal and dielectric layers, respectively. The reflectivity curve of the N-layer Kretschmann configuration model can be expressed as [30].

$$\begin{pmatrix} U_1 \\ V_1 \end{pmatrix} = M \begin{pmatrix} U_{N-1} \\ V_{N-1} \end{pmatrix} \tag{8}$$

where: (U_1, V_1) and (U_{N-1}, V_{N-1}) are the borderline terms of the 1st and Nth layers of electromagnetic fields. Equation 9 represents the characteristic matrix [30],

$$\prod_{K=2}^{N-1} M_K = \begin{pmatrix} M_{11} & M_{12} \\ M_{21} & M_{22} \end{pmatrix} \tag{9}$$

where:

$$M_K = \begin{pmatrix} \cos\beta_k & -\frac{i\sin\beta_k}{q_k} \\ -iq_k \sin\beta_k & \cos\beta_k \end{pmatrix} \tag{10}$$

$$q_k = \frac{\sqrt{\epsilon_k - n_1^2 \sin\theta_1^2}}{\epsilon_k} \tag{11}$$

$$\beta_k = \frac{2\pi d_k}{\lambda}\left(\sqrt{\epsilon_k - n_1^2 \sin\theta_1^2}\right) \tag{12}$$

The thickness of the $d_k$layer is denoted by k_{th}-layer, θ_k and λ represent the incident angle and wavelength of the incident light, respectively. Consequently, the complex reflection coefficient (r_p) is expressed as follows:

$$r_p = \left[\left(M_{11} + M_{12}q_5\right)q_1 - \frac{\left(M_{21} + M_{22}q_5\right)}{\left(M_{11} + M_{12}q_5\right)q_1} + \left(M_{21} + M_{22}q_5\right)\right] \tag{13}$$

The reflectivity (R_p) is obtained by,

$$R_p = \left|r_p\right|^2 \tag{14}$$

Several essential sensing parameters are involved in sensing applications, including the angular shift sensitivity (S) which is given by:

$$S = \frac{\Delta\theta_{SPR}}{\Delta n_s}[\text{deg.RIU}^{-1}] \tag{15}$$

where $\Delta\theta_{SPR}$ represents the SPR angle shift and Δn_s denotes the refractive index change.

Numerical Model

The proposed SPR sensor model was designed and analyzed using COMSOL Multiphysics based on the finite element method, as illustrated in Fig. 2. A 2D geometry was constructed, consisting of a glass prism/Ag layer (55 nm)/graphene (0.34 nm)/water configuration. Illumination of the Ag layer was achieved using a light source with a wavelength of 633 nm directed onto the top of the glass prism. To

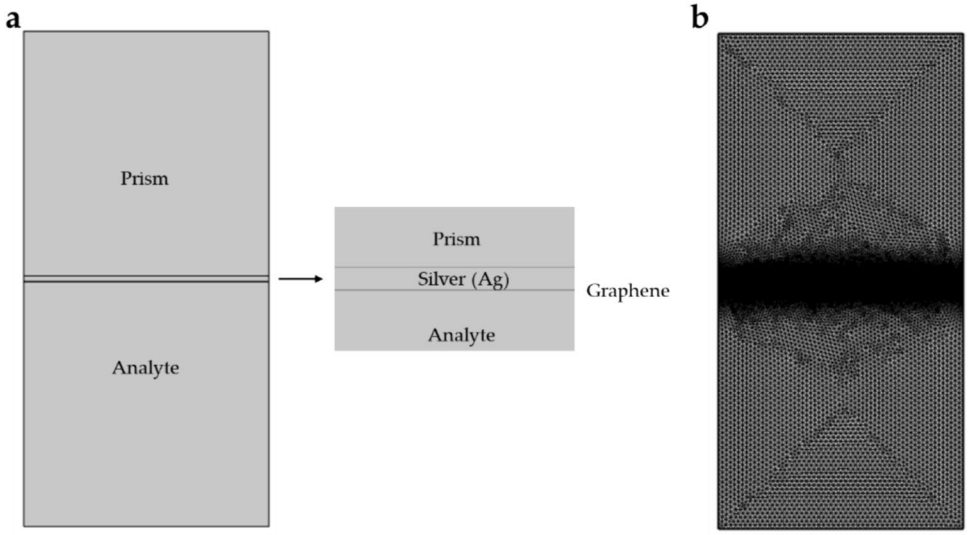


Fig. 2 Multiphysics view of the proposed SPR biosensor. **a** Numerical simulation model showing the proposed structure. **b** Computational mesh domain

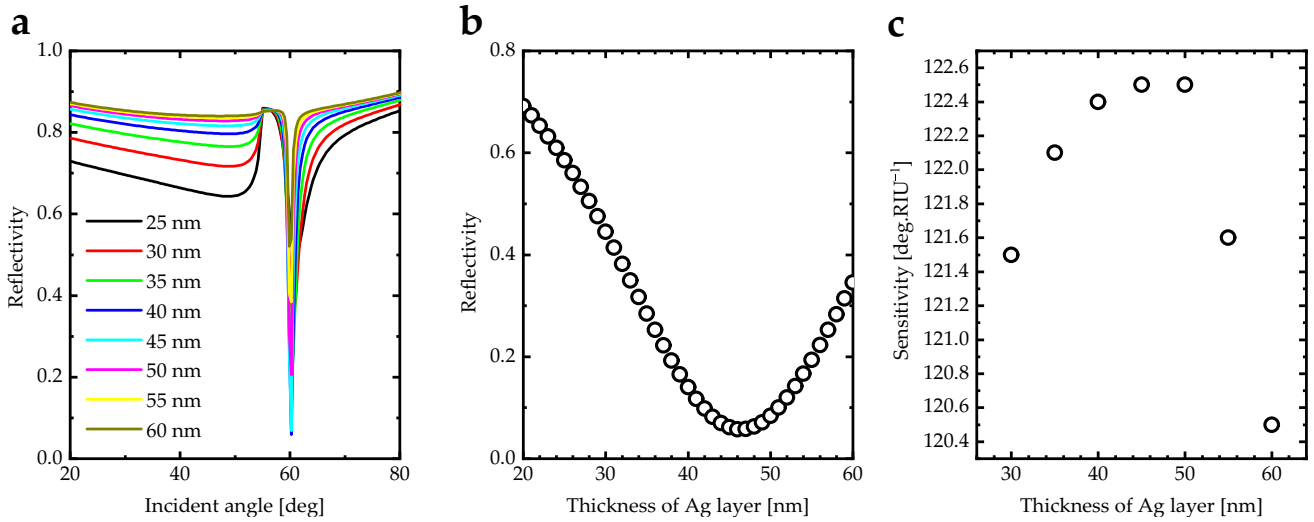


Fig. 3 **a** Reflectance of the Ag layers plotted against the resonance angles of the biosensor design, **b** Reflectance curves of the biosensor design with varying Ag-layer thicknesses, and **c** Sensivity of the bio-sensor as a function of the Ag-layer thickness

effectively simulate the sensor, Floquet periodic boundary conditions and periodic port conditions were implemented. Free triangular meshes with an element size ranging from 6.09×10^{-5} µm to 0.03 µm was employed. Moreover, the incident light angle from 40° to 89° in increments of 0.1° were varied. Additionally, the incident light angle was varied from 40° to 89° in increments of 0.1° to capture a comprehensive range of responses.

Results and Discussion

The parameters of the SPR-based biosensor model were optimized across varying thicknesses of the Ag layer. In Fig. 3a, reflectance curves for different Ag layer thicknesses are shown. As the Ag layer thickness increases from 20 nm to 40 nm, there is a noticeable shift in the resonance angle from 61.06° to 59.85°. Figure 3b indicates that the minimum

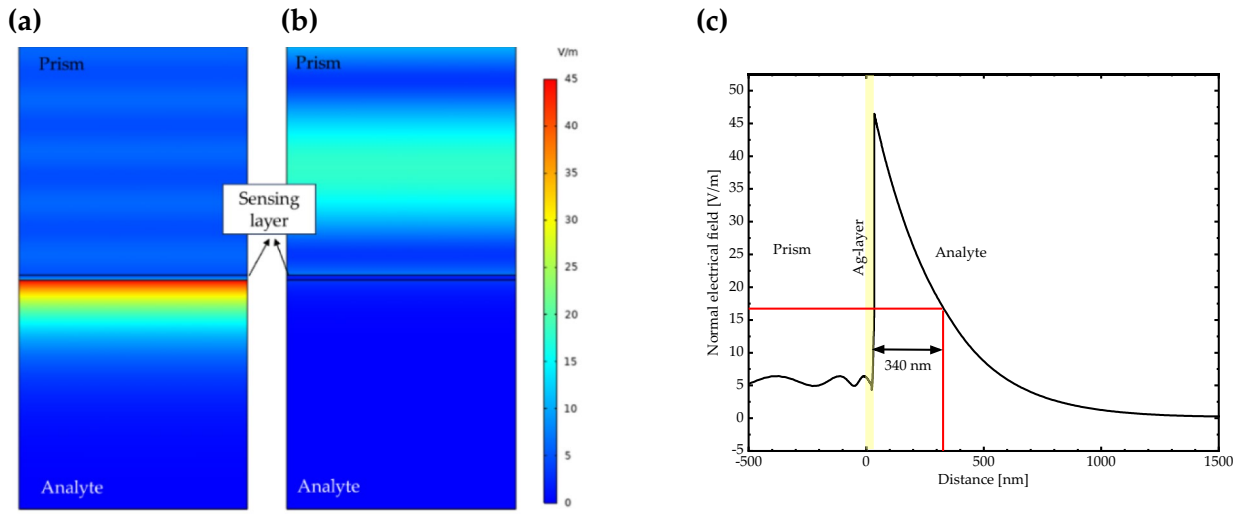


Fig. 4 Electric field norm distribution and magnetic field propagation in the proposed prism/Ag-layer/graphene sensor. **a** Electric field distribution at a non-resonance angle showing no enhanced field on the surface of silver (Ag). **b** Electric field distribution at a resonance angle exhibiting an enhanced field on the surface of silver (Ag). **c** Cross-section of the total electric field perpendicular to the prism base at the resonance angle, revealing a clear evanescent field at the sensing interface

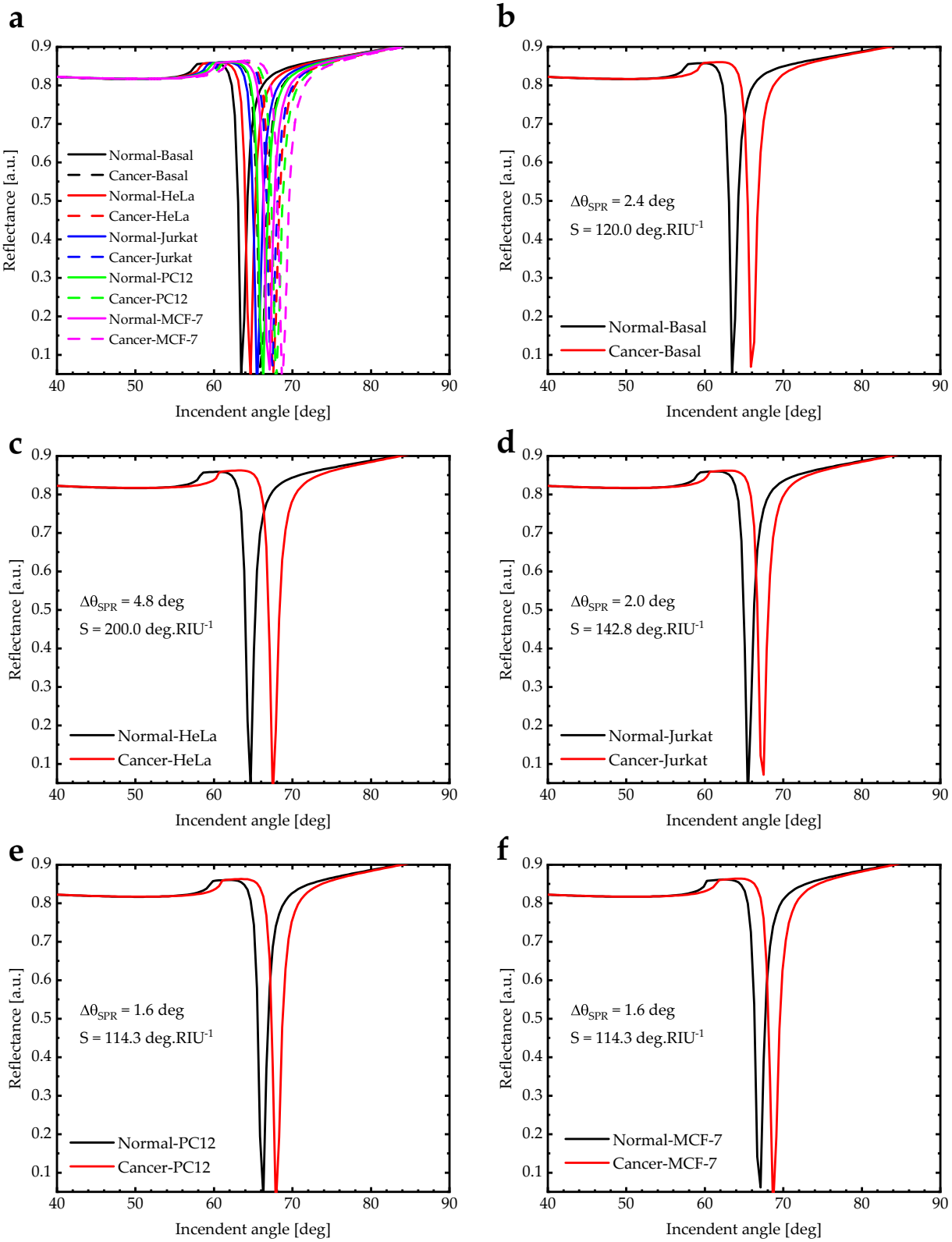


Fig. 5 **a** SPR curves of Basal, HeLa, Jurkat, PC12, and MCF-7 normal and cancerous cells. Sensing performance for different types of cells: **b** Basal, **c** HeLa, **d** Jurkat, **e** PC12, and **f** MCF-7

Table 2 Performance parameters comparing Basal, HeLa, Jurkat, PC12, and MCF-7 cancerous cells with normal cells

Cell name	Cell and density level	n [34, 35]	R_{min}	θ_{SPR} [deg.]	S [deg/RIU]
Basal	Normal cell (30–70%)	1.360	0.048	63.5	Ref.
	Skin cancer (80%)	1.380	0.069	65.9	120.0
HeLa	Normal cell (30–70%)	1.368	0.043	64.7	Ref.
	Cervical cancer (80%)	1.392	0.017	69.5	200.0
Jurkat	Normal cell (30–70%)	1.376	0.01	65.5	Ref.
	Blood cancer (80%)	1.390	0.072	67.5	142.9
PC12	Normal cell (30–70%)	1.381	0.037	66.3	Ref.
	Adrenal gland cancer (80%)	1.395	0.012	67.9	114.3
MCF-7	Normal cell (30–70%)	1.387	0.062	67.1	Ref.
	Breast cancer (80%)	1.401	0.008	68.7	114.3

reflectance at the resonance angle occurs at a thickness of 45 nm for the Ag layer. Sensitivity (S) of the biosensor was calculated using Eq. 15 for different Ag layer thicknesses and refractive index values of the analyte ranging from 1.33 to 1.41 with a step increment of 0.02. Figure 3c demonstrates that the highest sensitivity, reaching 122.5 deg/RIU, is achieved for Ag layer thicknesses within the range of 40–50 nm.

The electric field distribution in Fig. 4a and b shows a significant increase in field intensity at the sensing surface during resonance conditions, indicating a notable enhancement in electric field strength. In Fig. 4c, the prism/Ag/graphene sensor demonstrates an enhanced distribution of electric field norm and magnetic field propagation, particularly on the plasmonic Ag layer during resonance, indicative of intensified field strength under these conditions, as commonly observed in resonance phenomena [31].

Furthermore, the intensity of the electric field decreases exponentially within the medium containing the target biomolecules. The penetration depth (PD), which is defined as the distance traveled by the field perpendicular to the layer where the field intensity decreases to 1/e (37%), was calculated [32, 33]. For the prism/Ag/graphene SPR sensor, an optimized PD of 340 nm was determined, indicating a larger interaction volume of the field within the sensing medium. As a result, the electric probing field near the graphene layer exhibits high intensity and sensitivity to biomolecule interactions.

In Fig. 5a, SPR curves are shown for various types of normal and cancer cells, where solid lines represent normal cells and dashed lines represent cancer cells of the same type. Sensing performance is further detailed in Fig. 5(b-f). The minimum reflectance of Basal (skin cancer) cells occurs at 63.5° and 65.9° for normal and cancer cells, respectively (Fig. 5b), resulting in an SPR angle shift of 2.4° due to cancer. For HeLa (cervical cancer) cells, the minimum reflectance is observed at 64.7° and 69.5° for normal and cancer cells, respectively (Fig. 5c), indicating an SPR angle shift of 4.8°. Similarly, for Jurkat (blood cancer) cells, the minimum reflectance occurs at 65.5° and 67.5° for normal and cancer cells, respectively (Fig. 5d), with an SPR angle shift of 2.0°. For PC12 (adrenal gland cancer) cells, the minimum reflectance is at 66.3° and 67.9° for normal and cancer cells, respectively (Fig. 5e), corresponding to an SPR angle shift of 1.6°. Lastly, for MCF-7 (breast cancer) cells, the minimum reflectance is observed at 67.1° and 68.7° for normal and cancer cells, respectively (Fig. 5f), resulting in an SPR angle shift of 1.6°. Overall, the designed model effectively detects cancer in Basal, HeLa, Jurkat, PC12, and MCF-7 cells. Table 2 summarizes the recorded data for detecting different types of cancer cells, showing a maximum sensitivity of 200.0 deg/RIU for detecting HeLa cells and a minimum sensitivity of 114.3 deg/RIU for detecting PC12 and MCF-7 cells.

Conclusions

This study introduces a highly sensitive SPR biosensor configured with layers (glass prism/Ag/graphene) capable of operating effectively across a wide range of analyte refractive indices (1.33 to 1.41), enabling the detection of diverse biological solutions with varying refractive index characteristics. Furthermore, the SPR sensor demonstrates direct detection capability for cancerous cells in blood samples. The optimized thickness of the Ag plasmonic material contributes to enhanced sensor performance. Notably, the sensor shows a sensitivity of 120.0 deg/RIU for skin cancer cells, 200.0 deg/RIU for cervical cancer cells, 142.9 deg/RIU for blood cancer cells, and 114.3 deg/RIU for both adrenal gland and breast cancer cells. Given the promising results obtained, the proposed model holds significant potential for a wide range of bio-sensing applications.

Acknowledgements This work was supported and funded by the Deanship of Scientific Research at Imam Mohammad Ibn Saud Islamic University (IMSIU) (grant number IMSIU-RP23036).

Author Contributions S.A.: Conceptualization, Methodology, Software, Data curation, Writing – original draft, Visualization, Writing – review & editing, Resources. H.F.: Resources, Investigation, Data curation. A.A.: Data curation, Visualization, Investigation, Data curation, Writing – original draft.C.T.: Investigation, Writing – review & editing. A.T.: Conceptualization, Visualization, Investigation, Data curation, Writing – original draft, Validation, Supervision.

Funding Section additionally, the financial support was provided from the Deanship of Scientific Research at Imam Mohammad Ibn Saud Islamic University (IMSIU) under grant number IMSIU-RP23036.

Data Availability Data will be made available on request.

Declarations

Competing Interests The authors declare no competing interests.

References

1. Crosby D, Bhatia S, Brindle KM, Coussens LM, Dive C, Emberton M, Esener S, Fitzgerald RC, Gambhir SS, Kuhn P, Rebbeck TR, Balasubramanian S (2022) Early detection of cancer. Science 375(6586):eaay9040. https://doi.org/10.1126/science.aay9040. Epub 2022 Mar 18. PMID: 35298272.
2. Fitzgerald RC, Antoniou AC, Fruk L et al (2022) The future of early cancer detection. Nat Med 28:666–677. https://doi.org/10.1038/s41591-022-01746-x
3. Ramer R, Hinz B (2008) Inhibition of cancer cell invasion by cannabinoids via increased expression of tissue inhibitor of matrix metalloproteinases-1. JNCI: J Natl Cancer Inst 100(1):59–69
4. Yaroslavsky AN et al (2012) High-contrast mapping of basal cell carcinomas. Opt Lett 37(4):644–646
5. Cailleau R, Young R, Olive M, Reeves W Jr (1974) Breast tumor cell lines from pleural effusions. J Natl Cancer Inst 53(3):661–674
6. Mostufa S, Akib TBA, Rana MM, Islam MR (2022) Highly sensitive TiO2/Au/graphene layer-based surface plasmon resonance biosensor for cancer detection. Biosensors 12(8):603
7. Hossain B, Paul AK, Islam MA, Rahman MM, Sarkar AK, Abdulrazak LF (2022) A highly sensitive surface plasmon resonance biosensor using SnSe allotrope and heterostructure of BlueP/MoS2 for cancerous cell detection. Optik 252:168506
8. Masson J-F (2017) Surface plasmon resonance clinical biosensors for medical diagnostics. ACS Sens 2(1):16–30
9. Xue T et al (2019) Ultrasensitive detection of miRNA with an antimonene-based surface plasmon resonance sensor. Nat Commun 10(1):1–9
10. Dai X, Liang Y, Zhao Y, Gan S, Jia Y, Xiang Y (2019) Sensitivity enhancement of a surface plasmon resonance with tin selenide (SnSe) allotropes. Sensors 19(1):173
11. Bochenkov VE, Frederiksen M, Sutherland DS (2013) Enhanced refractive index sensitivity of elevated short-range ordered nanohole arrays in optically thin plasmonic au films. Opt Express 21(12):14763–14770
12. Yadav A, Sudhanva S, Sharan P, Kumar A (2021) Modeling, simulation and computational analysis of plasmonic optical sensor using BaTiO 3 in diabetes mellitus. Int J Inform Technol 13:2163–2168
13. Nguyen HH, Park J, Kang S, Kim M (2015) Surface plasmon resonance: a versatile technique for biosensor applications. Sensors 15(5):10481–10510
14. Wang D et al (2019) Recent advances in surface plasmon resonance imaging sensors. Sensors 19(6):1266
15. Yadav A, Mishra M, Tripathy SK, Kumar A, Singh O, Sharan P (2023) Improved surface plasmon effect in Ag-based SPR biosensor with graphene and WS2: an approach towards low cost urine-glucose detection. Plasmonics 18(6):2273–2283
16. Chen S, Hu S, Wu Y, Deng D, Luo Y, Chen Z (2021) Ultrasensitive biosensor with hyperbolic metamaterials composed of silver and zinc oxide. Nanomaterials 11(9):2220
17. Yadav A, Kumar A, Sharan P, Mishra M (2023) Highly sensitive bimetallic-metal nitride SPR biosensor for urine glucose detection. IEEE Trans Nanobiosci
18. Yadav A, Kumar A, Sharan P (2022) Sensitivity enhancement of a plasmonic biosensor for urine glucose detection by employing black phosphorous. JOSA B 39(1):200–206
19. Song B, Li D, Qi W, Elstner M, Fan C, Fang H (2010) a highly conductive material with excellent adsorption properties for high-resolution bio/nanodetection and identification. ChemPhysChem 11(3):585–589
20. Artiles MS, Rout CS, Fisher TS (2011) Graphene-based hybrid materials and devices for biosensing. Adv Drug Deliv Rev 63(14–15):1352–1360
21. Banerjee AN (2018) Graphene and its derivatives as biomedical materials: future prospects and challenges. Interface Focus 8(3):20170056
22. Lou J, Cheng T, Li S, Zhang X (2019) Surface plasmon resonance photonic crystal fiber biosensor based on gold-graphene layers. Opt Fiber Technol 50:206–211
23. Yadav A, Sharan P, Kumar A (2020) Surface plasmonic resonance based five layered structure-biosensor for sugar level measurement in human. Results Opt 1:100002
24. Rahman MM, Rana MM, Rahman MS, Anower M, Mollah MA, Paul AK (2020) Sensitivity enhancement of SPR biosensors employing heterostructure of PtSe2 and 2D materials. Opt Mater 107:110123
25. Akib TBA et al (2021) Design and numerical analysis of a graphene-coated SPR biosensor for rapid detection of the novel coronavirus. Sensors 21(10):3491
26. Ouyang Q et al (2016) Sensitivity enhancement of transition metal dichalcogenides/silicon nanostructure-based surface plasmon resonance biosensor. Sci Rep 6(1):28190
27. Bruna M, Borini S (2009) Optical constants of graphene layers in the visible range. Appl Phys Lett, 94, 3
28. Shalabney A, Abdulhalim I (2011) Sensitivity-enhancement methods for surface plasmon sensors. Laser Photonics Rev 5(4):571–606
29. Kim S-H, Koh K (2006) Functional dyes for surface plasmon resonance-based sensing system. Functional dyes. Elsevier, pp 185–213
30. Maurya J, Prajapati Y, Singh V, Saini J, Tripathi R (2015) Performance of graphene–MoS 2 based surface plasmon resonance sensor using silicon layer. Opt Quant Electron 47(11):3599–3611
31. Dey B, Islam MS, Park J (2021) Numerical design of high-performance WS2/metal/WS2/graphene heterostructure based surface plasmon resonance refractive index sensor. Results Phys 23:104021
32. Maurya JB, François A, Prajapati YK (2018) Two-dimensional layered nanomaterial-based one-dimensional photonic crystal refractive index sensor. Sensors 18(3):857
33. Zeng S et al (2015) Graphene–MoS2 hybrid nanostructures enhanced surface plasmon resonance biosensors. Sens Actuators B 207:801–810

34. Chopra H, Kaler RS, Painam B (2016) Photonic crystal waveguide-based biosensor for detection of diseases. J Nanophotonics 10(3):036011–036011
35. Sani MH, Khosroabadi S (2020) A novel design and analysis of high-sensitivity biosensor based on nano-cavity for detection of blood component, diabetes, cancer and glucose concentration. IEEE Sens J 20(13):7161–7168

Publisher's Note Springer Nature remains neutral with regard to jurisdictional claims in published maps and institutional affiliations.

Springer Nature or its licensor (e.g. a society or other partner) holds exclusive rights to this article under a publishing agreement with the author(s) or other rightsholder(s); author self-archiving of the accepted manuscript version of this article is solely governed by the terms of such publishing agreement and applicable law.